IOPscience iopscience.iop.org

Home Search Collections Journals About Contact us My IOPscience

# Thermal etching defect structures on Si(001): a comparative study with high-resolution low-energy electron diffraction and scanning tunnelling microscopy

This article has been downloaded from IOPscience. Please scroll down to see the full text article.

1995 J. Phys.: Condens. Matter 7 5313

(http://iopscience.iop.org/0953-8984/7/27/016)

View the table of contents for this issue, or go to the journal homepage for more

Download details:
IP Address: 171.66.16.151
The article was downloaded on 12/05/2010 at 21:38

Please note that terms and conditions apply.

J. Phys.: Condens. Matter 7 (1995) 5313–5326. Printed in the UK

# Thermal etching defect structures on Si(001): a comparative study with high-resolution low-energy electron diffraction and scanning tunnelling microscopy

A W Munz†, W Weiss‡ and W Göpel†

† Institut für Physikalische und Theoretische Chemie, Universität Tübingen, Auf der Morgenstelle 8, D-7400 Tübingen, Germany
‡ Fritz-Haber-Institut der Max-Planck-Gesellschaft, Faradayweg 4–6, D-14195, Berlin, Germany

Received 4 January 1995, in final form 19 April 1995

**Abstract.** Defect structures formed on Si(001) surfaces heated to different temperatures were studied comparatively with a high-resolution spot profile analysis low-energy electron diffraction (LEED) system and with a scanning tunnelling microscope. Using scanning tunnelling microscopy (STM) we observed tetragonal pyramids after annealing the surface to 1400 K which are formed by a thermal etching process that removes silicon from the surface. With increasing slope of the pyramid planes we observe a transformation from monatomic to $D_B$ double steps. For the latter, dimer rows of the $(2\times1)$ reconstruction extend perpendicular to the step edges. Pyramid planes with $D_B$ double steps that are rotated by 90° transform into each other by the formation of single-stepped planes. For annealing temperatures of 1600 K, very flat surfaces with only monatomic steps are formed. A profile analysis of the specular and half-order beams of the two-domain Si(001) $(2\times1)$ LEED pattern was performed after the same preparation procedures were applied to the samples. This analysis leads to step structures that are identical with the results from the real-space STM studies.

## 1. Introduction

Since the first low-energy electron diffraction (LEED) [1,2], reflection high-energy electron diffraction (RHEED) [3] and scanning tunnelling microscopy (STM) [4] studies on Si(001), this technologically important surface is still the subject of intensive surface science investigations. Because of its high reactivity the results of these investigations can be strongly influenced by differences in the individual UHV equipment and by slight differences in the preparation procedure. At room temperature, the surface atoms on Si(001) form dimers, thereby creating $(1\times2)$ and $(2\times1)$ reconstructed domains that are separated by monatomic steps $a_0/4$ high, where $a_0 = 0.543$ nm is the cubic lattice constant of silicon. However, other structures beside the $(2\times1)$ structure [5] were observed on this surface, depending on the sample temperature and surface impurities. These are $(2\times2)$ [6], $c(4\times2)$ [7,8] and $(2\times n)$ [9,10] reconstructions. The theoretically predicted asymmetric dimers [11] of the $(2\times1)$ structure were observed by STM [12,13]. Mass transport [14] and surface diffusion on this surface [15] were studied by several workers.

The surface atoms of the $(2\times1)$ and $(1\times2)$ domains rotated by 90° belong to the two FCC sublattices of the diamond structure. On a $(1\times2)$ domain the dimer rows run along the [110] direction perpendicular to the upper terminating step edge which is denoted as $S_B$ (single step B [16]), and on a $(2\times1)$ domain the dimer rows run along $[\bar{1}10]$ parallel

to the terminating upper $S_A$ step edge as can be seen later in figure 4. The height of a monatomic step is $d = 0.136$ nm. The corresponding double steps are denoted $D_B$ and $D_A$. There is increasing interest in the investigation of the assumed phase transition from single-stepped ($S_A + S_B$) to double-stepped ($D_B$) vicinal Si(001) surfaces, which should depend on the temperature $T$ and the tilt angle $\gamma$, the latter describing the miscut angle between the corresponding surface plane and the (001) plane [17]. This is important because the antiphase domain structure of single-stepped *Si(001)* surfaces causes problems in the growth of heteroepitaxial structures onto this substrate such as GaAs/Si [18, 19], whereas high-quality epitaxial films can be obtained on double-stepped substrate surfaces exhibiting only one domain. The above phase transition was studied theoretically by several groups [17, 20–22]. They predict a first-order phase transition which, however, could not be verified experimentally so far. In contradiction, RHEED and LEED as well as STM [23] measurements indicate a gradual transition that excludes a first-order process. Because the LEED [24, 25] and RHEED [26] results do not clarify how this gradual transition depends on $T$ *and* $\gamma$, the discussion about this point is still going on.

In the past, most work on Si(001) was primarily focused on its intrinsic properties. Because of the high reactivity of this surface, reproducible experimental conditions to reveal these intrinsic properties are difficult to achieve. The enormous influence of small amounts of contamination (e.g. Ni) on the surface reconstruction has been demonstrated for example for the formation of the Si(001) $(2 \times n)$ phases [10]. In this paper we present results on the atomic step structures and the surface topography in the micrometre range of Si(001) surfaces that were annealed to temperatures between 1400 and 1600 K. The results of a previous LEED beam profile analysis [27, 28] are reviewed in section 3.1. They are in line with the STM results presented in section 3.2. New results about the transition from $S_A + S_B$ single-stepped to $D_B$ double-stepped surfaces are obtained. We also discuss the influence of contamination on the step structures formed during the thermal preparation procedure. They probably play an important role even if their coverage is near or below the limits of x-ray photoelectron spectroscopy (XPS) detection (1%).

In a STM study the influence of contamination was previously reported by Dijkkamp *et al* [29] and the step structure of artificial gratings was described by Umbach *et al* [14]. Our results are in line with these studies but in addition we can follow the contamination-induced gradual transition from single- to double-stepped faces and we are able to determine the creation of low-indexed facets on an atomic scale. Furthermore a comparison of spot profile analysis (SPA) LEED and STM data is given.

## 2. Experimental details

The LEED experiments were performed in a separate ultrahigh-vacuum (UHV) chamber equipped with a high-resolution SPA LEED instrument, which has been described in detail in [28]. It allows us to record spot profiles by scanning the diffracted LEED beams over a channeltron detector with a small aperture using electrostatic deflection. The coherence length of our instrument is about 100 nm as determined on a $(7 \times 7)$-reconstructed Si(111) surface. This allows us to detect steps which occur with an average distance of up to 100 nm on the surface. In our experiments the intensity profiles of the specular beam were recorded at an angle of incidence 3.75° with respect to the surface normal, which is due to the geometry of the instrument [28].

The base pressure in the UHV chamber was $2 \times 10^{-10}$ mbar. Si(001) wafers 15 mm × 10 mm in size and highly P doped ($10^{16}$ cm$^{-3}$) were ultrasonically cleaned

in methanol and mounted onto the manipulator. They were clamped between two tantalum holders which allowed direct heating of the wafers. After brief (1 min) sputtering with 500 eV $Ne^+$ to remove carbon contamination from the surface the samples were annealed to about 1000 K to remove the oxide layer. Annealing temperatures were determined with a pyrometer, calibrated at 970 K against a Ni–(Ni–Cr) thermocouple. After the samples were heated for 5–10 min to the elevated temperature, they were rapidly cooled to room temperature and the LEED measurements were performed. We have used this preparation procedure in other UHV systems and found impurity signals below the detection limits of XPS and ultraviolet photoelectron spectroscopy (UPS). However, small impurity concentrations after long measurement times and repeated heating cycles cannot be ruled out.

The STM experiments were carried out in an ion-pumped UHV chamber with a base pressure of less than $1.0 \times 10^{-10}$ mbar. The commercially available scanning tunnelling microscope has been described in detail elsewhere [30]. All STM images were recorded in the constant-current mode (CCM). The STM tips were made by electrochemical etching of tungsten wires. The phosphorus-doped (0.5 Ω cm) Si samples (25 mm × 7 mm × 0.5 mm) were ultrasonically rinsed in ethanol. After they were transferred into the vacuum chamber, the *in situ* preparation was started by outgassing the samples and the sample holder for about 10 h at 800 K to maintain a low base pressure during subsequent thermal cleaning. To remove the native oxide layer the samples were heated resistively to 1400 or 1600 K. The maximum temperature during one preparation cycle was held for only a few seconds. The increase and decrease in the temperature were carried out rapidly. This procedure was performed in a manipulator cooled with liquid nitrogen which caused the pressure to stay in the $10^{-9}$ mbar range.

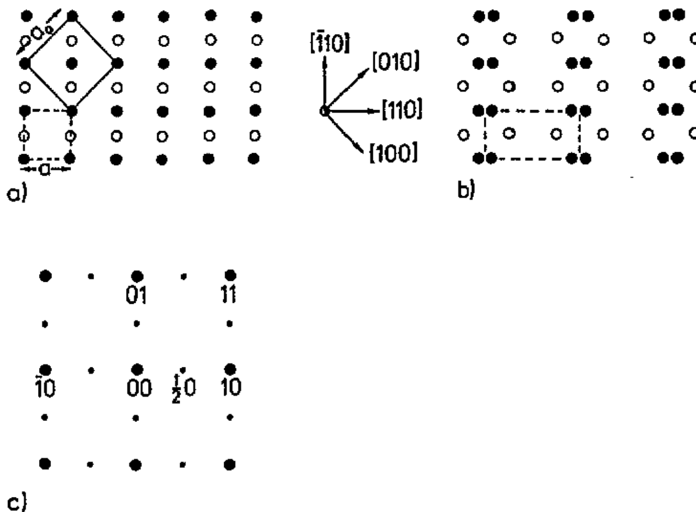


**Figure 1.** Schematic view (*a*) of the unreconstructed Si(001) surface and (*b*) of the (2 × 1) reconstructed surface; the top-layer atoms are denoted by the full circles, and the second-layer atoms by open circles. $a_0 = 0.543$ nm is the cubic lattice constant of silicon and $a = 0.348$ nm is the spacing of the two-dimensional unit cell of the unreconstructed Si(001) surface. The height of a monatomic step is $d = 0.136$ nm. In (*c*), the two-domain LEED pattern is shown schematically.

## 3. Results

### 3.1. *Spot profile analysis low-energy electron diffraction measurements*

We always observe a two-domain LEED pattern shown schematically in figure 1(*c*) resulting from coexisting $(1 \times 2)$ and $(2 \times 1)$ reconstructed domains on the surface that are separated by monatomic steps. The unreconstructed and the $(2 \times 1)$ reconstructed Si(001) surfaces are shown schematically in figures 1(*a*) and 1(*b*).

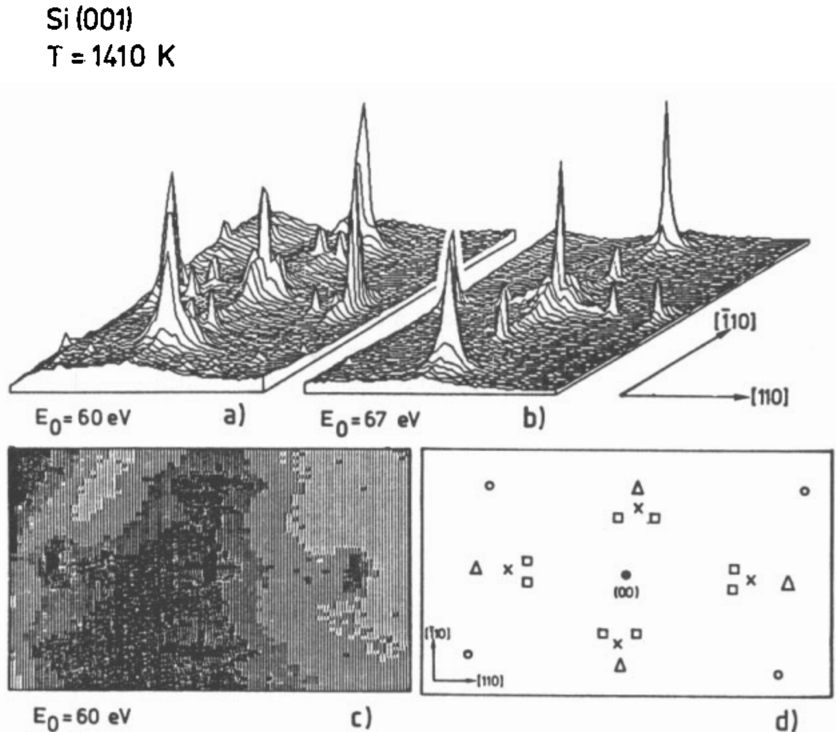


**Figure 2.** Experimentally observed LEED intensity contours for primary electron energies of (*a*) 60 eV and (*b*) 67 eV. The map taken at 60 eV is displayed also in a grey-scale plot in (*c*) and schematically in (*d*): $\Delta$, half-order spots of Si(001) $(2 \times 1)$; $\times$, integral order spots of Si(113) $(3 \times 1)$; $\bullet$, $\frac{1}{3}$-order spots of Si(113) $(3 \times 1)$; $\bigcirc$, half-order spots of Si(001) p$(2 \times 2)$.

In figures 2(*a*) and 2(*b*) the LEED patterns at two different electron energies of a Si(001) surface that was heated repeatedly to $T = 1410$ K are shown. The pattern in figure 2(*a*) is shown on a grey-scale plot in figure 2(*c*) and in a schematic diagram in figure 2(*d*). The main contributions around the specular beam are due to the half-order spots of the $(1 \times 2)$ and $(2 \times 1)$ reconstructions (open triangles in figure 2(*d*)). Additional spots appear in between the specular beam and the first half-order spots (crosses and full circles in figure 2(*d*)). They result from $(3 \times 1)$ reconstructed (113) facets that occur in a fourfold symmetry as discussed in more detail in [28]. They presumably form the upper parts of tetragonal pyramids on the Si(001) surface as will be discussed later.

In figure 3, the intensity profiles of the specular beam at different electron energies are shown, each of them extending over half a Brillouin zone from $k_{\parallel} = -\pi/2a$ to $+\pi/2a$. $k_{\parallel}$

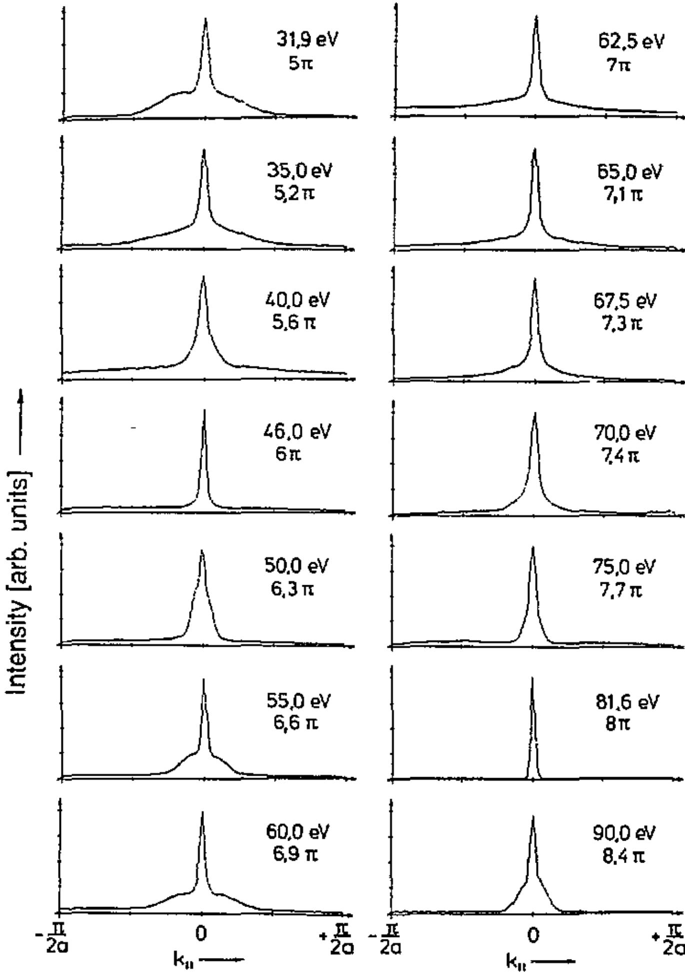


**Figure 3.** Intensity profiles of the specular beam along the [110] direction. For each primary electron energy the phase difference $k_{\perp}2d$ is indicated.

is the component of the electron scattering vector $\boldsymbol{k}$ parallel to the surface and $a$ is the lattice constant of the two-dimensional unit cell on the unreconstructed Si(001) surface as discussed above. Also, for each profile the phase difference $\Delta\phi = k_{\perp}2d$ of electrons scattered from (001) terraces separated by double steps is indicated, where $k_{\perp}$ is the component of the electron scattering vector $k$ perpendicular to the surface and $d$ is the height of a monatomic step on Si(001). If this phase difference is an integer multiple of $2\pi$ ($\Delta\phi = 2\pi, 4\pi, \ldots$), these terraces scatter in phase and a sharp spot is obtained. If the phase difference is an odd multiple of $\pi$ ($\Delta\phi = \pi, 3\pi, \ldots$) these terraces scatter out of phase and a spot splitting or a spot broadening is obtained [31].

The profiles under out-of-phase scattering conditions in figure 3 clearly can be separated into a sharp spot and a broad shoulder. The full widths at half-maximum (FWHMs) of these difference parts show different behaviours as a function of $k_{\perp}d$. We measured the FWHM of the narrow part of the profile as a function of the electron energy for the (00), (10) and (11) beams. For the preparation temperature of 1410 K these FWHM oscillations indicate

the coexistence of the monatomic, diatomic and up to eight-atom steps on the Si(001) surface [27]. Although the intensity profile is created by the entire step structure on the surface and the broad shoulder cannot be analysed completely separately from the sharp part, the broad shoulder mainly reflects the existence of short periodicities in terms of small terraces. Therefore we now want to concentrate on the broad shoulder of the intensity profile in order to learn about the step heights and step directions that create these small terraces. As can be seen in figure 3, the broad shoulder shows a maximum FWHM at the out-of-phase scattering conditions for double steps ($\Delta\phi = 5\pi, 7\pi, \ldots$), and a sharp profile is obtained at the in-phase scattering conditions ($\Delta\phi = 6\pi, 8\pi, \ldots$). From the maximal FWHM $\Delta k_{\|}/k_{10} = 10\%$ at the out-of-phase energies the average distance between double steps is about ten lattice constants. The LEED pattern taken at $E = 60$ eV displayed in the grey-scale plot in figure 2(*c*) corresponds to a phase shift $\Delta\phi = k_{\perp}2d = 6.9\pi$ for the (00) beam and to $\Delta\phi = 7.22\pi$ for the $(\frac{1}{2}, 0)$ and $(0, \frac{1}{2})$ beams, which both are close to out-of-phase scattering conditions for double steps. It can be seen that the specular beam is broadened mainly along the [110] and [$\bar{1}$10] directions, which is due to double-step edges running along these directions on the surface. Theoretical total-energy calculations reveal formation energies of $\lambda(D_A) = (0.54 \pm 0.01\ \mathrm{eV})/a$ for a double step where the dimer rows run parallel to the step edge and $\lambda(D_B) = (0.05 \pm 0.02\ \mathrm{eV})/a$ for a double step where the dimer rows run perpendicular to the step edge [16]. Both half-order spots in figure 2(*c*) ($(\frac{1}{2}, 0)$ and $(0, \frac{1}{2})$) show a broadening along the direction perpendicular to the twofold periodicity of the $(1 \times 2)$ and $(2 \times 1)$ superstructure unit cells. This means that the broadening of the specular and the half-order beams is caused by the $D_B$ double steps with the dimer rows running perpendicular to the upper terminating step edges. It further shows that there are no double steps running along the [100] and [010] directions, which implies that along these directions $(1 \times 2)$ and $(2 \times 1)$ terraces separated by $D_B$ double steps must transform into each other via the formation of single steps. This was also observed in a recent SPA LEED investigation [34] and it can be seen directly in the STM images presented in the next section. We only measured the profile of the specular beam systematically as a function of $k_{\perp}2d$. The LEED pattern in figure 2(*b*) taken at $E = 67$ eV corresponds to a phase shift $\Delta\phi = k_{\perp}2d = 7.62\pi$ that is already closer to an in-phase scattering condition than the LEED pattern at 60 eV. It can be clearly seen that here the FWHM of the broad shoulder of the specular beam and of the half-order beams has decreased.

From this we conclude that $D_B$ double steps with the dimer rows running perpendicular to the step edges occur along the [110] and [$\bar{1}$10] directions ($\langle 110 \rangle$) with an average distance of ten lattice constants (about 3 nm). They form tetragonal pyramids on the surface as can be seen in the STM images presented in the nest section. Along the [100] and [010] directions ($\langle 100 \rangle$) the $(1 \times 2)$ and $(2 \times 1)$ terraces separated by $D_B$ double steps are transformed by single-stepped planes. If we heat the samples to higher temperatures, we observe different step structures with no multiple steps present any longer. Heating the sample first to 1400 K and afterwards to 1600 K results in only small FWHM variations in the (00) beam, indicating the existence of monatomic steps with an average distance of 40 nm corresponding to a misorientation angle $\gamma = 0.2°$. After heating samples with no misorientation ($\gamma = 0°$) to 1600 K for the first time we obtain very flat surfaces with no detectable steps any longer, indicating an average terrace size of more than 100 nm [27]. These observations are in line with the results obtained from the STM experiments that are presented below.

### 3.2. *Scanning tunnelling microscopy measurements*

Figure 4 shows a stepped Si(001) surface with coexisting $(1 \times 2)$ and $(2 \times 1)$ reconstructed domains, which was obtained after heating to 1600 K. On a $(1 \times 2)$ domain the dimer rows

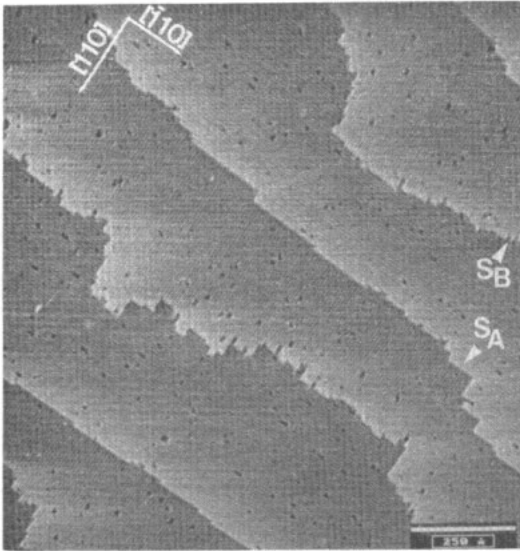


**Figure 4.** Recording of the alternating domain structure on single-stepped vicinal Si(001) that was heated to 1600 K. The crystallographic directions are indicated. A (2 × 1) domain is terminated by an upper $S_A$ step; the rough $S_B$ step terminates a (1 × 2) domain (scan size, 100 nm × 100 nm; sample voltage, 1.25 V; current, 0.9 nA).

run along [110] perpendicular to the terrace-terminating single step ($S_B$). On a (2 × 1) domain the rows run along [$\bar{1}$10] parallel to the terrace-terminating single step ($S_A$). The crystallographic directions are indicated. The record shows the well known surface structure of Si(001).

The four STM images in figure 5(*a*) were obtained after heating the sample to 1400 K. The imaged surface areas are separated by several tens of micrometres. The coverage of the surface by contamination (we assume that it is SiC [32]) is below 2%, which was estimated by calculating the area around the top of the pyramids. This coverage may be below the detection limit of XPS. The contamination is randomly distributed on the surface and acts as pinning centres for step edges running around the contamination; thus pyramids of tetragonal shape and prismatic structures in between these pyramids were built up. The created structures can be explained by a thermal etching process that takes place during the preparation procedure (heating to 1400 K). The velocity of the step edge shift caused by thermal etching and therefore the formation of the rough surface topography should depend on parameters such as heating temperature, heating time, crystallographic directions on the surface, the formation energies of the different step edges ($S_A$, $S_B$, $D_B$ and $D_A$), step–step interaction, surface diffusion and the arrangement and chemistry of the contaminations. This will be discussed below.

First we want to describe the two borderline cases of the arrangement of two interacting next-neighbour pinning centres. If the line connecting two pinning centres is along a ⟨100⟩ direction, the terraces in between these two pinning centres become very narrow and remain rudimentary as bottleneck structures labelled bn in figure 5(*b*). If the etching process proceeds via bottleneck structures (figure 5(*b*)), separated terraces on the same height with individual geometrical centres will be created. Each centre point migrates towards the corresponding pinning centre and finally remains at the pinning site. The terrace is then part of the pyramid and creates a new basal pyramid plane. If the connection line between two

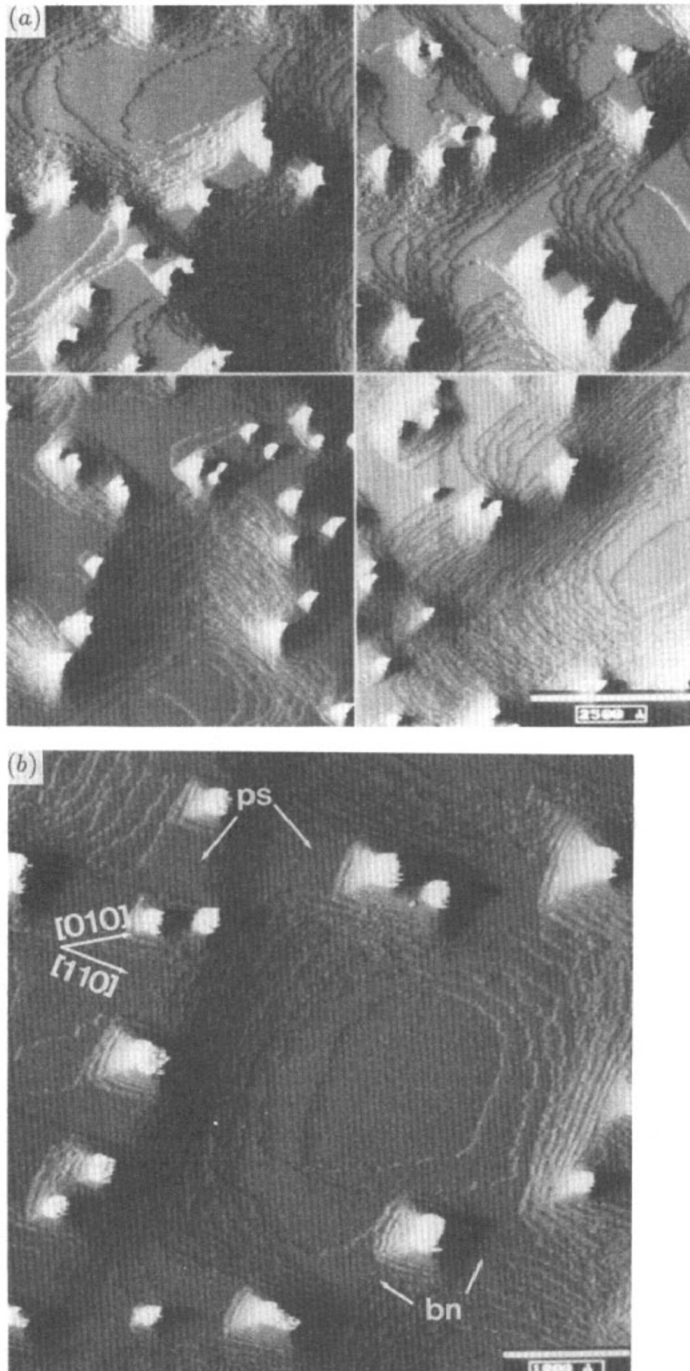


**Figure 5.** (*a*) Four STM images of vicinal Si(001), taken from wide (50 $\mu$m) separated areas of the surface after annealing for a few seconds at 1400 K. Randomly separated areas of contaminations appear as bright spots. The crystallographic directions and the scale are indicated (scan size (4×), 510 nm × 510 nm; sample voltage, 1.25 V; current, 0.9 nA). (*b*) Image of vicinal Si(001). The image shows prismatic structures (ps) along $\langle 110 \rangle$ and bottleneck structures (bn) along $\langle 010 \rangle$ directions (scan size, 510 nm × 510 nm; sample voltage, 1.25 V; current, 0.9 nA).

pinning centres is along a ⟨110⟩ direction, the terraces show a tendency to have orthogonal shapes, thereby forming prismatic structures labelled ps in figure 5(*b*). In this case the geometrical centre of the terrace remains in between the two pinning centres. This general behaviour leads to tetragonal pyramids with orthogonal prismatic etching structures along the ⟨110⟩ directions and bottleneck structures along the ⟨100⟩ directions in between.

In figure 6(*a*) the step edge formation of a prismatic plane which is aligned along the $[\bar{1}10]$ direction is shown. From the lower right (etch pit) to the upper left along the solid line a gradual reduction in the $(2 \times 1)$ domain area from layer to layer is observable. In the upper left part near the pinning site, only $D_B$ double steps occur. The $D_B$ double steps show an increasing density towards the pinning centre. This is equivalent to a gradual change in the slope and therefore the local tilt angle, which can be seen in figure 6(*b*) showing the step profile along the line in figure 6(*a*). Figure 6(*b*) also reveals the gradual transition from a single (right side) to a $D_B$ stepped surface area (left side). Between A and B along the solid line of the step profile in figure 6(*a*) the edges predominantly consist of $D_B$ double steps and the number of $S_A + S_B$ single steps is very small. The average width of the terraces between A and B is about 3 nm which corresponds to $7a$ or $8a$ ($a = 0.348$ nm). This result is in agreement with the average distance between $D_B$ double steps as determined by LEED. The $w$-index of the imaged $[uvw]$ directions in figure 6(*a*) decreases towards the pinning centre. The lowest index in figure 6(*a*) is $w = 7$ (corresponding to the region around A). Profiles of other areas not shown exhibit terraces belonging to $w = 5$. The inclination angles of the (115) and (117) faces are 15.79° and 11.42°, respectively. For geometrical reasons, atomic imaging by STM on faces with higher slopes is difficult. The stable (113) [33] surface for example has an inclination angle of 25.2° with respect to the (001) surface. In this work we observe $(3 \times 1)$ reconstructed (113) facets with LEED that occur with fourfold symmetry on the surface and probably form the uppermost parts of the pyramid planes. These parts could not be imaged by STM, presumably because of the large tilt angle of the small areas around the top of the pyramids.

In figure 6(*c*) the step structure along a ⟨100⟩ direction is shown for a region where the step edges make a curve, thereby changing their direction by 90° from the $[\bar{1}10]$ to the [110] direction. On the left side of figure 6(*c*) we observe smooth $S_A$ step edges and rough $S_B$ step edges, both running along the $[\bar{1}10]$ direction which is the diagonal of the image (from the lower left to the upper right corner). On the left side of the image the ratio of $(1 \times 2)$ and $(2 \times 1)$ domain areas is greater than unity, similar to the area between the centre and the upper left side of figure 6(*a*). Figure 6(*a*) is taken in the region of the extended diagonal of the lower left side of figure 6(*c*). On the right side of figure 6(*c*) the step edges make a curve and change their direction by 90° from the $[\bar{1}10]$ to the [110] direction. In the region after a direction change of 45° the $(1 \times 2)$ to $(2 \times 1)$ domain area ratio is about unity and the only single steps with a high kink density occur. Along these directions, no double steps were observed by LEED, either. This confirms that the formation of $D_B$ double steps and $S_A + S_B$ single steps depends on the azimuthal direction on the surface [34].

In figure 6(*d*) a sequence of step profiles along the [110] direction (profiles a–c) is shown. It describes schematically the formation of a double-stepped plane and includes characteristic step profiles that were formed temporarily during the thermal etching process. On the left side of the sequence an invariant contamination and on the right side the direction of the step flow is indicated. Profile a shows a pure single-stepped surface with $S_A$ and $S_B$ step edges and a nearly constant ratio of $(1 \times 2)$ to $(2 \times 1)$ domain areas of unity. The profile of the vicinal surface shows the macroscopic tilt angle. In profile b a transition stage is shown. One dotted line displays the shift during the thermal etching of a step edge from profile a to a new position in profile b and also from profile b to profile c. The

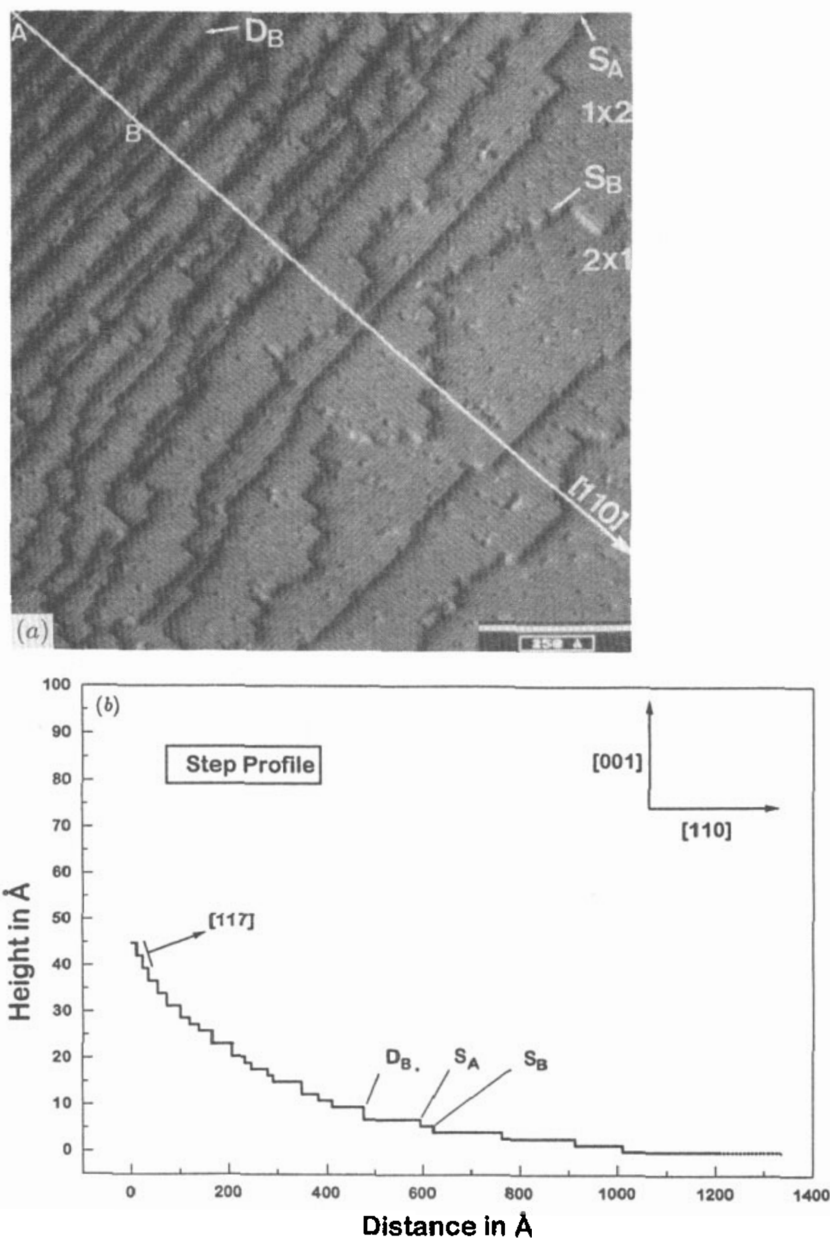


**Figure 6.** (*a*) STM image of Si(001). The record shows a magnification of a 1400 K pre-treated sample. Single-layer ($S_{A,B}$) and double-layer ($D_B$) steps appear. The dimer rows indicate the (2 × 1) and (1 × 2) domains. The indicated line is running along the [110] direction (scan size, 105 nm × 105 nm; sample voltage, 1.29 V; current, 2.9 nA). (*b*) Step profile along the indicated line in (*a*). At the top a (116) face is indicated. On the right side of the profile, only single steps occur, and towards the left side a transition from single to double steps occurs. The upper left side only consists of $D_B$ double steps. (*c*) On the right side of the image the step formation on a plane along the [100] direction is shown, where only $S_A$ and $S_B$ single steps with high kink densities appear (scan size, 105 nm × 105 nm; sample voltage, 1.29 V; current, 2.9 nA). (*d*) Schematic sequence of step profiles a, b and c. From profile a to profile c the contamination-induced formation of double-stepped faces during the thermal etching is shown.

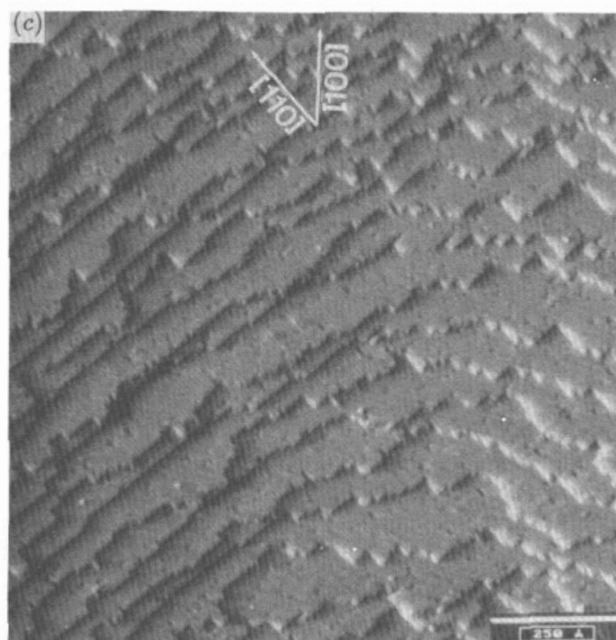


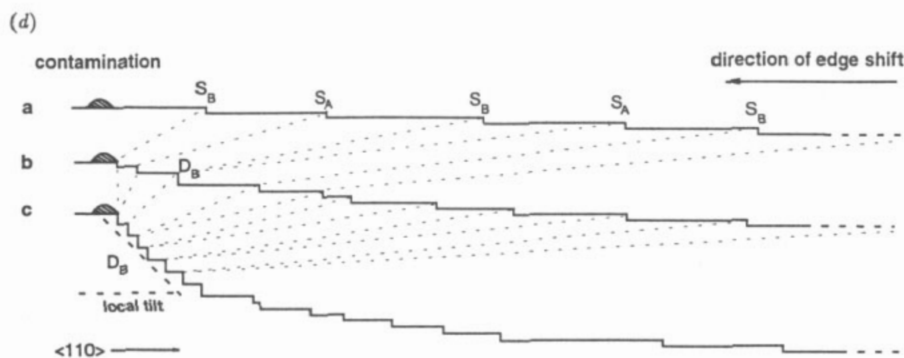


**Figure 6.** (Continued)

thermal etching process starts with profile a. The edges shift towards the contamination. The contamination prohibits the evaporation of the first underlying silicon layer, thereby pinning them (profile b). This causes (if the thermal etching proceeds) an increasing step density and local tilt angle towards the pinning centre. The $S_A$ step edges shift more rapidly than the $S_B$ step edges until they reach the next $S_B$ step edge. Then a $D_B$ double step is formed (profile b). The velocity of the $D_B$ step edge shift decreases compared with the $S_A$ and $S_B$ step edge shift velocities. The density of $D_B$ steps around a pinning centre is increased. Finally (profile c) the low-indexed double-stepped faces, e.g. (117), occur (see figures 6(*a*) and 6(*b*)).

$S_A$ and $S_B$ steps are only defined in the ⟨110⟩ directions. Between two ⟨110⟩ directions the step edges consist of different numbers of $S_A$ and $S_B$ step segments. Their numbers depend on the direction of the edge. Because step edges along the ⟨100⟩ directions consist

of equal numbers of $S_A$ and $S_B$ segments, no geometric and energy diffrences between two next-neighbour edges exist and they have equal shift velocities. Therefore the single-stepped vicinal faces along this direction are conserved (see figure 6(*c*)) during the thermal etching procedure.

If the preparation temperature is increased to 1600 K, no contamination acting as nuclei for terrace pinning remains on the surface and the vicinal single-stepped surface in figure 4 is obtained. This is the same sample as recorded in figure 6(*a*) but heated in a second preparation cycle to $T = 1600$ K. The tilt angle of the vicinal surface in figure 4 is 0.23° towards the [110] azimuth, and only single steps were observed on this surface. This was also observed by LEED.

## 4. Discussion

Now we want to discuss the influence of different factors on the formation of the Si(001) surface topography [35] that we observe after heating the samples. As mentioned before, these factors are surface diffusion [15, 36], step–step interaction [22, 37] and step formation energies [38, 39]. They influence the velocity of the step edge shift caused by thermal evaporation of silicon and therefore the surface topography formed after the etching procedure.

Mo *et al* [15] found that the atomic diffusion on Si(001) surfaces is highly anisotropic, because the migration of Si atoms along the dimer rows is much more rapid than perpendicular to them. $S_B$ steps appear as good symmetrical sinks for downward- and upward-migrating adatoms but $S_A$ step edges do not [36]. However, the experiments reported were carried out at temperatures between 350 and 550 K and simple extrapolations to temperatures up to 1400 K are not possible. However, the influence of surface diffusion cannot be ignored because when cooling the samples to room temperature the above-mentioned temperature range is passed through.

Because the contamination prohibits the thermal layer-by-layer etching, it causes locally an increase in the step edge density. In some areas of the surface (around the contamination) the terrace width is reduced to less than $10a$ (figure 5(*b*)). It is known that $S_B$ and $D_B$ steps have dipoles [22] which interact when the distance between neighbouring step edges becomes small [37]. There is a repulsive force between B-type step edges and an attractive force between the B- and A-type step edges. Therefore a reduction in $(2 \times 1)$ domains takes place. The dipole forces also enhance the shift of the $S_A$ step edges and reduce it for the $S_B$ step edges.

Another important factor is the step formation energies. The first total-energy calculations performed by Chadi [16] revealed that $\lambda(S_A) = 0.02$ eV$/2a$, $\lambda(S_B = 0.3$ eV$/2a$ and $\lambda(D_B) = 0.05$ eV$/2a$. According to this, the $\lambda(S_B)/\lambda(S_A)$ ratio is 15. Experimental investigations by Mo *et al* [36] and Swartzentruber *et al* [39] revealed ratios of about three. The measurements were carried out on vicinal Si(001) surfaces with rather large terrace widths (25 nm). If the step formation energies were the dominant factor determining the step flow during the heating procedure, we should expect a preferential growth of $(2 \times 1)$ domains on our samples because of the higher formation energy of $S_B$ steps than of $S_A$. On the rough surfaces we could not find any indication that $(2 \times 1)$ domains preferentially remained, indicating a $(1 \times 2)$ to $(2 \times 1)$ formation energy ratio of the order of unity. Webb [35] pointed to the energetically subordinated role of formation energies compared with the Si–Si bond energies which are more than ten times higher. We conclude that, for the high-temperature etching, the influence of the step formation energy on the step edge

shift velocities and therefore on the surface topography is small when compared with the influence of the bond energies, surface diffusion and step–step interactions.

If the evaporation rate is sufficiently high (at 1600 K), single-stepped surfaces are formed. At lower preparation temperatures (1400 K), contamination can be avoided. The interplay between thermal etching and the distribution of contamination is responsible for the formation of the rough surface topography. Along the ⟨110⟩ directions the terrace pinning leads locally to increasing step densities, the creation of double steps and gradual transitions from single- to double-stepped facet planes. In these areas, step–step interaction, surface diffusion and step formation energies influence the velocity of the step edge shifts. They are responsible for the local topography finally created. Because step edges along the ⟨100⟩ directions consist of nearly equal numbers of $S_A$ and $S_B$ segments, next-neighbour edges shift with the same velocities along these directions. This is the reason why single-stepped facet planes along the ⟨100⟩ directions are conserved during the etching procedure.

## 5. Summary

The step and topographic structures on Si(001) surfaces prepared by heating to different temperatures were investigated by a LEED beam profile analysis and by STM. The results obtained from both techniques are in line with each other. For preparation temperatures of 1400 K the LEED measurements reveal the coexistence of monatomic, diatomic and up to eight-atom steps and the formation of (113) facets. $D_B$ double steps were observed only along the ⟨110⟩ directions, where the dimer rows run perpendicular to the step edges. The average terrace width between these double steps is 0.3 nm. Along the ⟨100⟩ directions, only single steps and no double steps were detected by LEED.

These steps form tetragonal pyramids that were imaged directly by STM. In between these pyramids, orthogonal prismatic structures with steps along the ⟨110⟩ directions and bottleneck-like structures with steps along the ⟨100⟩ directions are formed, depending on the direction of the line connecting two neighouring pyramids. These topographic structures are created by a thermal etching process that removes silicon from the surface during the annealing procedure. On the top of the pyramids, contamination acts as pinning centres that are not removed by the thermal etching procedure when heating the samples to 1400 K.

With increasing slope towards the pinning centres a transformation from single to $D_B$ double steps is observed with STM along the ⟨110⟩ directions. The step density and the slope of the plane increase towards these pyramid centres, leading to (117), (115) and possibly (113) facet planes. $D_B$ double-stepped planes along the ⟨110⟩ directions that are rotated by 90° are transformed via single-stepped planes along the ⟨100⟩ directions. Along the ⟨100⟩ directions the single-step edges have a high kink density.

After heating the Si(001) surface to 1600 K only single steps were observed and the terrace width corresponds to the misorientation of the sample surface towards the (001) plane. Presumably the contamination that acts as pinning centres, thereby creating the pyramid structures at an annealing temperature of 1400 K, was removed after heating the samples to 1600 K.

## Acknowledgments

We would like to thank W Ranke for reading the manuscript and helpful discussions, and D Schmeisser and Ch Ziegler for useful discussions. The STM work was supported in part by the Deutsche Forschungsgemeinschaft, Bonn, by the grant Go 301/20-1.

## References

[1] Appelbaum J A and Hamann D R 1978 *Surf. Sci.* **74** 21
[2] Seiwatz R 1964 *Surf. Sci.* **74** 473
[3] Sakamoto T, Kawai N J, Nakagawa T, Ohta K and Kojima T 1985 *Appl. Phys. Lett.* **47** 617
[4] Tromp R M, Hamers R J and Demuth J E 1985 *Phys. Rev. Lett.* **55** 1303
[5] Schlier R E and Farnsworth H E 1957 *Semiconductor Surface Physics* ed R H Kingston (Philadelphia, University of Pennsylvania Press) p 3
[6] Cardillo M J and Becker G E 1978 *Phys. Rev. Lett.* **40** 1148; 1980 *Phys. Rev.* B **21** 1497
[7] Lander J J and Morrison J 1962 *J. Appl. Phys.* **33** 2089; 1962 *J. Chem. Phys.* **37** 729
[8] Poppendieck T D, Gnoc T C and Webb M B 1978 *Surf. Sci.* **75** 28
[9] Martin J A, Savage D E, Moritz W and Lagally M G 1986 *Phys. Rev. Lett.* **56** 1936
[10] Niehus H, Köhler U K, Copel M and Demuth J E 1988 *J. Microsc.* **152** 735
[11] Chadi D J 1979 *Phys. Rev. Lett.* **43** 43
[12] Sugihara K, Sakai A, Kato Y, Akama Y, Shoda N, Tokumoto H and Ono M 1990 *J. Vac. Sci. Technol.* B **9** 707
[13] Wiesendanger R, Bürgler D, Tarrach G, Güntherodt H-J, Shvets I V and Coey J M D 1992 *Surf. Sci.* **274** 93
[14] Umbach C C, Keeffe M E and Blakely J M 1991 *J. Vac. Sci. Technol.* A **9** 1014; 1991 *J. Vac. Sci. Technol.* B **9** 721; 1993 *J. Vac. Sci. Technol.* A **11** 1830
[15] Mo Y-W, Kleiner J, Webb M B and Lagally M G 1992 *Surf. Sci.* **268** 275
Mo Y-W and Lagally M G 1991 *Surf. Sci.* **248** 313
[16] Chadi D J 1987 *Phys. Rev. Lett.* **59** 1691
[17] Alerhand O L, Nihat Beker A, Joannopoulos J D, Vanderbilt D, Hamers R J and Demuth J E 1990 *Phys. Rev. Lett.* **64** 2406
[18] Kroemer H 1986 *Heteroepitaxy on Silicon (Mater. Res. Soc. Symp. Proc. 67)* ed J C C Fan and J M Poate (Pittsburgh, PA: Materials Research Society) p 3
[19] Aspes D E and Ihm J 1986 *Phys. Rev. Lett.* **57** 3054
[20] Alerhand O L, Nihat Beker A, Joannopoulos J D, Vanderbilt D, Hamers R J and Demuth J E 1991 *Phys. Rev. Lett.* **66** 1991
[21] Bartelt N C, Einstein T L and Rottman C 1990 *Phys. Rev. Lett.* **66** 961
[22] Poon T W, Yip S, Ho P S and Abraham F F 1990 *Phys. Rev. Lett.* **65** 2161
[23] Itoh H, Narui S, Zhang Z and Ichonokawa T 1992 *Surf. Sci. Lett.* **277** L70
[24] Tong X and Bennett P A 1991 *Phys. Rev. Lett.* **67** 101
[25] Schröder-Bergen E and Ranke W 1991 *Surf. Sci.* **259** 323
[26] de Miguel J J, Aumann C E, Kariotis R and Lagally M G 1991 *Phys. Rev. Lett.* **67** 2830
[27] Weiss W, Schmeisser D and Göpel W 1988 *Phys. Rev. Lett.* **60** 1326
[28] Weiss W, Schmeisser D and Göpel W 1989 *Surf. Sci.* **207** 401
[29] Dijkkamp D, van Loenen E J, Hoeven A J and Dieleman J 1990 *J. Vac. Sci. Technol.* A **8** 218
Dijkkamp D, Hoeven A J, van Loenen E J, Lenssinck J M and Dieleman J 1989 *Appl. Phys. Lett.* **56** 39
[30] Besocke K 1987 *Surf. Sci.* **181** 145
[31] Gronwald K D and Henzler M 1986 *Surf. Sci.* **117** 441
[32] Ishikawa Y, Ikeda N, Kenmochi M and Ichinokawa T 1985 *Surf. Sci.* **159** 256
[33] Ranke W and Xing Y R 1985 *Phys. Rev.* B **31** 2246
[34] Wasserfall J and Ranke W 1994 *Surf. Sci.* **315** 227
[35] Webb M B 1994 *Surf. Sci.* **299** 454 and references therein
[36] Mo Y-W, Schwartzentruber B S, Kariotis R, Webb M B and Lagally G 1989 *Phys. Rev. Lett.* **63** 2393
[37] Pehlke E and Tersoff J 1991 *Phys. Rev. Lett.* **67** 465
[38] Qian Guo-Xin and Chadi D J 1986 *J. Vac. Sci. Technol.* B **4** 1079
[39] Swartzentruber B S, Mo Y-W, Kariotis R, Lagally M G and Webb M B 1990 *Phys. Rev. Lett.* **65** 1913